Step Scan Interferometry in the Mid-Infrared with Photothermal Detection

MATTHEW J. SMITH, CHRISTOPHER J. MANNING, RICHARD A. PALMER,* and JAMES L. CHAO

Department of Chemistry, P. M. Gross Chemical Laboratory, Duke University, Durham, North Carolina 27706 (M.J.S., C.J.M., R.A.P.); and IBM Corporation, Research Triangle Park, North Carolina 27709 (J.L.C.)

A medium resolution mid-infrared FT-IR instrument (IBM Instruments IR/44) has been modified to do step scanning; this has been done with the use of concepts previously applied to both near- and far-infrared instruments. In this paper we illustrate the method used for driving the mirror in the step scan mode and present some preliminary results from using the instrument with photothermal detection. At the current state of development, results obtained with the use of phase modulation indicate that this method produces significantly higher signal-to-noise ratios than does the use of amplitude (chopper) modulation to generate the photothermal signal.

Index Headings: **FT-IR; Photothermal beam deflection; Mirage effect; Photoacoustic; Phase modulation; Step scan interferometry.**

INTRODUCTION

Photothermal methods of detection, including photothermal beam deflection (mirage effect) and sample-gas-microphone photoacoustic detection, are now well-established techniques for condensed matter vibrational spectroscopy.[1-7] Because infrared dispersive instruments lack sufficient throughput, photothermal detection has been used almost exclusively with interferometric (FT-IR) spectrometers.[1,2] These instruments have the well-known inherent advantages of multiplexing, high throughput, and spectral indexing. However, with a rapid scanning interferometer, the intensity modulation of the source beam for photothermal detection is intrinsic to generation of the interferogram. As a consequence, each wavelength is modulated at a different (Fourier) frequency. Currently available FT-IR instruments (rapid scanning), even operating at the lowest available mirror velocities, generate Fourier frequencies ranging from ~100 to 1000 Hz for the region from 400 to 4000 cm^{-1} (mid-IR). In addition to their continuous change with wavelength, the range of these modulation frequencies is higher than desirable for photothermal detection. The relatively high modulation frequencies produce weak signal strength, and lack of constant modulation frequency precludes lock-in amplification. Furthermore, the thermal diffusion depth is different for each wavelength.[2,8] Lowering the mirror velocity by a factor of 10 is feasible and would seem useful, but, since lock-in amplification would still be unusable, the predicted S/N enhancement would be largely negated by low-frequency vibrations and 1/f noise, since they would be in the same range as the Fourier modulation frequencies.

In contrast, a step scan interferometer (1) accommodates any desired modulation frequency, (2) applies that frequency at all wavelengths, and (3) allows measurement with the use of a lock-in amplifier. The result is a single interferogram, created point by point, which is otherwise equivalent to that created by coaddition of rapid scanning interferograms.

The step scan method requires precise control of the position of the moving mirror.[9-15] As is also the case in modern rapid scanning interferometry, the sinusoidal interferogram of a HeNe laser is used to ensure that data points are collected at equal intervals of mirror position. In the rapid scan mode, these laser fringes provide trigger pulses for A/D signal conversion. Successive interferograms thus generated are coadded in order to increase S/N, before being Fourier transformed. However, in the step scan method, the mirror is stopped at each data collection point, where it is jittered at a constant frequency. The resulting phase modulation of the laser intensity is used in a feedback loop to control the position of the mirror. This jitter also creates a phase modulation in the intensity of the emerging IR radiation which (under proper circumstances) may be used to generate the photothermal signal. Alternatively, the IR beam may be intensity modulated externally (for example, with a chopper), with the phase modulation being used only for mirror control. In either case, a lock-in amplifier referenced to the frequency of intensity modulation is used to detect and amplify the signal at each data point, prior to digitization. Thus, for each FT-IR spectrum generated, only a single scan of the moving mirror (a single interferogram) is required. Signal-to-noise enhancement by signal averaging is achieved by accumulating data at each individual point for a longer time period.

In this paper we present an approach to the development of a mid-infrared step scan FT spectrometer. This approach uses concepts previously applied successfully to visible/near-infrared,[9,10,13,14] and far-

Received 25 January 1988.
* Author to whom correspondence should be sent.

0003-7028/88/4204-0546$2.00/0

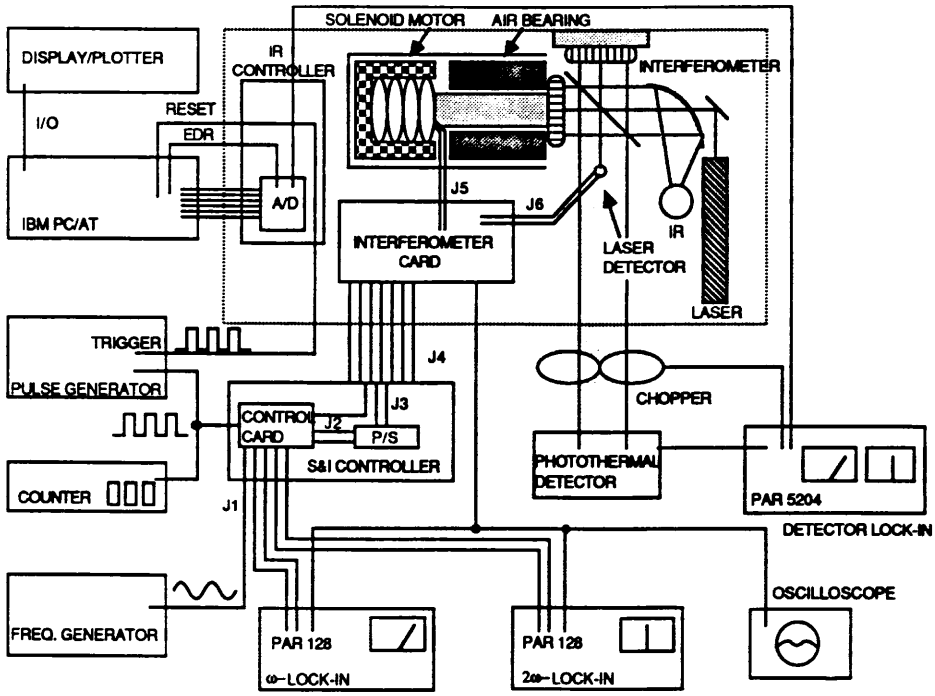

FIG. 1. Block diagram of step scan IR/44 instrument shown as configured for amplitude modulation photothermal spectrometry.

infrared[11,12,15] interferometry. The perfection of this step scan FT-IR instrument will increase the sensitivity, S/N, and versatility of photothermal detection methods in the IR by allowing the benefits of lock-in detection and optimum (low) modulation frequency to be exploited. While the results presented are preliminary, they do illustrate the potential of the technique.

EXPERIMENTAL

The step scan instrument is based on an IBM Instruments IR/44. For the results reported here, a second IR/44 has been used in its standard rapid scanning mode for comparison with the step scan results; however, the current design allows both rapid scan and step scan modes with the same instrument. The IR/44 is a nitrogen-purged benchtop FT-IR system employing a standard 45° Michelson interferometer with $f/4.2$ optics, a 7-W globar source, and a Ge-on-KBr beamsplitter. The data systems (for both the rapid scanning and step scanning IR/44 models) are IBM PC/AT's, each with an 80287 math coprocessor.

To accomplish step scanning with the IBM IR/44, we extensively modified the control circuit for the moving mirror. The modulation was achieved by incorporating mechanical viscous damping and an electronic feedback circuit into the control of the existing solenoid linear motor. This approach was adapted from the NIR/VIS instrument design described by Débarre *et al.*[9] A block diagram of the instrument is shown in Fig. 1.

The viscous damping is accomplished by a 30-mm × 15-mm aluminum paddle immersed in a 40-mm × 20-mm × 15-mm container of silicone fluid. The paddle is rigidly attached to the air bearing coil. The fluid, trimethylsiloxy-terminated polydimethylsiloxane (Petrarch Systems, Bristol, PA), is available in different viscosities, according to the average molecular weight of the polymer. Polymers of several viscosities were evaluated, ranging from 60,000 to 2,500,000 centistokes. The best results were achieved with the use of the 300,000 centistokes fluid.

The principle of the electronic feedback circuit used to drive the motor in a step-by-step fashion is related to that used in modern rapid scanning instruments. Although this theory has been previously discussed by Débarre *et al.*,[9,10] it is presented in greater detail here with respect to the way it relates to the current work. As in rapid scanning interferometry, a HeNe laser beam, passing through the optics of the interferometer and detected by a photodiode, provides the reference for data acquisition at equal intervals of optical retardation. The output voltage of the HeNe laser detector is a single frequency sinusoidal interferogram as the optical path difference is varied (Fig. 2). The voltage of the laser signal is given by:

$$V = \frac{V_0\{1 + \cos[2\pi\sigma\delta]\}}{2} \qquad [1]$$

where σ is the laser frequency (15,803 cm^{-1}), and δ is the optical path difference. In the usual rapid scanning experiment, data are collected whenever $V = V_0/2$. This occurs when the cosine term is zero, that is, at $\delta = n/\sigma$ or $n/2\sigma$ (every ½ wavelength of the HeNe laser interferogram).

On the other hand, to operate in the step scan mode, the mirror must be stopped at each data collection point, held at that point while data are collected, and then moved to the next point. The mirror position is controlled by a feedback loop which monitors the interference pattern of the HeNe laser (Fig. 2). The position is sensed by sinusoidal vibration of the moving mirror ("phase jitter") and detection of the resulting phase

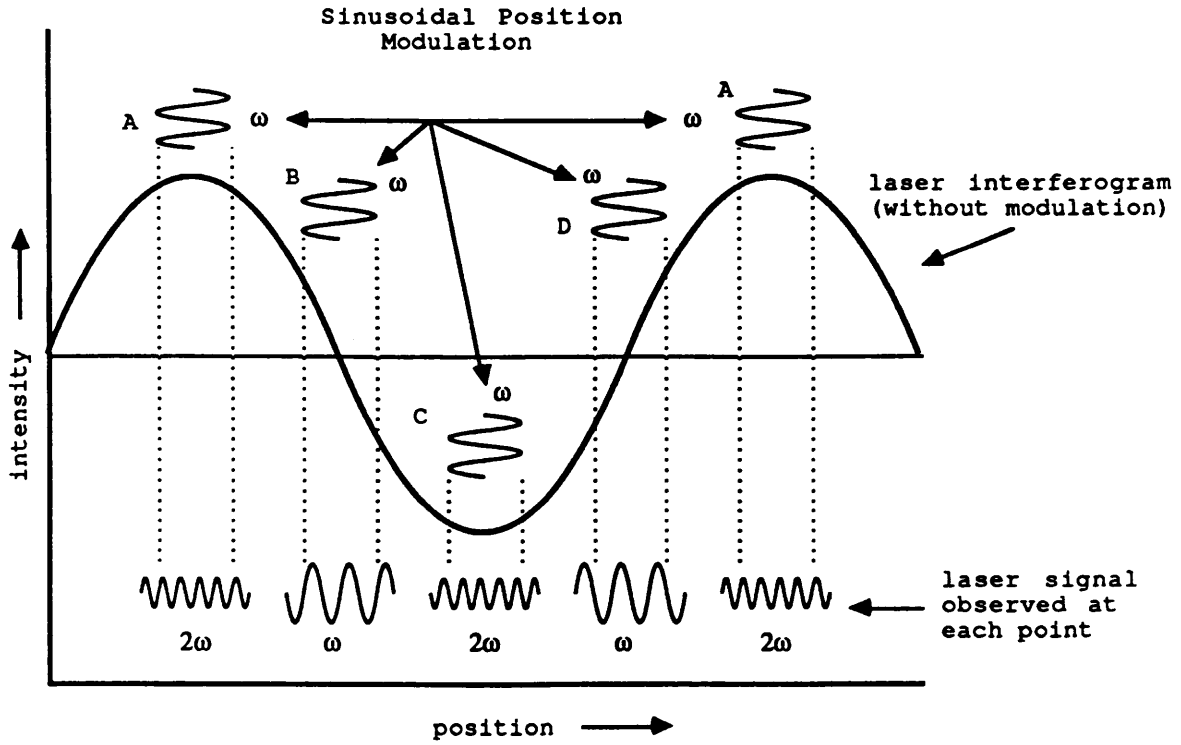

FIG. 2. Feedback control sequence for step scan interferometry. Points A, C: locked on extremum, ω minimized, 2ω maximized. Points B, D: locked on zero crossing, 2ω minimized, ω maximized.

modulation in the laser interference signal. Thus, as the mirror is vibrated back and forth at a constant frequency, the function which describes the HeNe laser detector output is:

$$V = \frac{V_0\{1 + \cos[2\pi\sigma(\delta + \epsilon \sin(\omega t))]\}}{2} \qquad [2]$$

where δ is the path difference (cm), ϵ is the amplitude of the phase modulation about δ (cm), σ is the energy of the laser (cm^{-1}), and ω is the modulation frequency (radians). This expression may be equivalently written as a Fourier series involving the harmonics of the $\sin(\omega t)$ term as follows:

$$\begin{aligned} V = V_0[&\tfrac{1}{2} + \tfrac{1}{2}J_0(2\pi\sigma\epsilon)\cos(2\pi\sigma\delta) && \text{[zero order]} \\ &-J_1(2\pi\sigma\epsilon)\sin(2\pi\sigma\delta)\cdot\sin(\omega t) && \text{[first order]} \\ &+J_2(2\pi\sigma\epsilon)\cos(2\pi\sigma\delta)\cdot\cos(2\omega t) && \text{[second order]} \\ &-J_3 \ldots && [3] \end{aligned}$$

where $J_x(2\pi\sigma\epsilon)$ is the Bessel function of order x. It is the first- and second-order terms which are important to the step scan control mechanism.

At interference extrema, the observed signal frequency is principally 2ω. At zero crossings, it is principally ω. At each position, one of the lock-in amplifiers is used to detect the minor component at that position, and its output is applied as feedback to minimize that component, thus holding the mirror in position. At alternate positions, the other lock-in is used. Thus, when the laser photodiode signal is input to the lock-in amplifier tuned to the ω-frequency, the lock-in will have an output proportional to $J_1(2\pi\sigma\epsilon)\sin(2\pi\sigma\delta)$. If $\delta = n/\sigma$ or $n/2\sigma$, corresponding exactly to the maxima and minima, respectively, of the laser interferogram (points A and C on Fig. 2), then the lock-in output voltage will be zero. Since the lock-in output is applied as feedback to the linear motor, it keeps the mirror's position locked on one or the other of these two positions. Any error signal caused by the mirror's drifting from the position on which it is fixed causes the lock-in signal to become nonzero and forces the mirror back to the locked position.

While the *first-order* term is nulled at n/σ and $n/2\sigma$, the *second-order* term is maximized at these positions. The second-order term varies as $+\cos(2\omega t)$, and has amplitude $+J_2(2\pi\sigma\epsilon)\cos(2\pi\sigma\delta)$. This term goes to zero when $\delta = n/4\sigma$ or $3n/4\sigma$. Thus, the output of a second lock-in amplifier tuned to 2ω is used as feedback to fix the mirror at these positions, which correspond to the zero crossings of the HeNe laser interferogram (points B and D on Fig. 2). Therefore, at any one position, a feedback signal is generated by one of the two lock-in amplifiers which drives the mirror to the desired position and holds it there during data collection.

Figure 2 shows how sequential stepping in the same direction is achieved. Starting at point A, the ω-signal is a minimum, and the 2ω-signal is a maximum. At this point, the ω-lock-in is used as feedback while data are collected. To step to point B, the control circuit then switches the feedback control to the 2ω-lock-in. This "pushes" the mirror to position B. At this point, the ω-signal is maximized, and the 2ω-signal is minimized. To step to point C, the circuit switches the phase of the ω-lock-in reference frequency by 180° before applying the ω-lock-in output as the feedback. The phase change is required in order to keep the mirror moving in the same direction on alternating steps. Thus, to step to point D, the 2ω-lock-in reference phase is changed by

180°, and then its output is applied as feedback. To complete the cycle, the reference phase of the ω-lock-in is changed back, and then *its* output is applied as feedback as the mirror steps to a new point A. Thus, by alternation of each lock-in and its reference phase as feedback control, the mirror is moved by ¼ λ_{HeNe} steps.

The effect of stepping by ¼ of the HeNe wavelength and collecting data at each point, rather than collecting every ½ λ_{HeNe} as most rapid scanning instruments do, is to increase the free spectral range from 15,800 cm^{-1} to 31,600 cm^{-1}. This means that one could use the instrument as a near-infrared/visible instrument by simply changing the source and beamsplitter[9] (and detector, if it were to be used for other than photothermal experiments). However, with the instrument configured for mid-infrared operation, the beamsplitter limits the optical throughput to the range 400 to ~5000 cm^{-1}. Since resolution is determined by how far the mirror travels, not by how closely the data points are spaced, no advantage is gained for use of the instrument in the IR by collection at every ¼ λ_{HeNe}; in fact, valuable time is wasted. Thus, for mid-IR operation, in order to reduce the time required to acquire the interferogram, one collects data only every *fourth* step (once per λ_{HeNe}). This uniquely describes a free spectral range of 7900 cm^{-1}.

For example, to collect data at λ_{HeNe} intervals, as described above, the computer sends the feedback control circuit three pulses in rapid succession, during which no data are collected. After driving the control circuit with a fourth pulse, and after a short delay (settling time, 50 ms or more), the computer then samples the A/D converter 2048 times during the preset sampling interval, typically 0.1–30 s. These 2048 A/D samples are averaged in order to improve signal-to-noise. (In addition, analog signal averaging is achieved by increasing the lock-in time constant.) The cycle is then repeated until an interferogram is acquired which will yield a spectrum of the desired resolution.

The step rate and data collection are controlled by the IBM PC/AT. The data collection routines of the standard IR/44 software were modified so that the computer generates pulses which are used to drive the feedback control switching circuit, which steps the mirror, and to sample the detector analog-to-digital (A/D) converter. Because the sequences used to drive the instrument are integral to the software, factors such as the total number of data points collected per interferogram, the undersampling ratio, the number of A/D samples per point, and the signal averaging time at each point are easily changed by keyboard commands.

The photoacoustic spectra illustrated were obtained with the use of a Princeton Applied Research Corp. Model 6003 photoacoustic cell with an accompanying PAR 6005 amplifier/power supply. A 35-mm off-axis paraboloid mirror was used to turn the collimated infrared beam of the IR/44 by 90° and focus it downward onto the sample through a ZnSe window. For the step-and-integrate experiments, the output of the PAR photoacoustic cell was fed into a PARC Model 5204 two-phase lock-in analyzer. The Model 5204 allows for simultaneous measurement of the in-phase and quadrature components of the photoacoustic signal and has outputs for the direct measurement of the magnitude and phase angle.

RESULTS

A direct comparison between step scanning and rapid scanning with the use of photothermal detection is illustrated in Fig. 3. Figure 3A is the step scan sample-gas-microphone photoacoustic spectrum of carbon black at 8-cm^{-1} resolution. This was obtained from the collection (over a period of 1.5 h) and Fourier transformation of 2048 interferogram points with the use of a 300 ms lock-in time constant and a chopper modulation frequency of 50 Hz. The spectrum obtained by step scanning is to be compared with the rapid scanning spectrum shown in Fig. 3B. We obtained the rapid scanning spectrum by coadding 512 single scan 2048 point interferograms (8-cm^{-1} resolution) collected in ~4 min. The rapid scanning optical velocity, 0.31 cm/s, yielded photothermal modulation frequencies in the range 1500 Hz at 4800 cm^{-1} to 120 Hz at 400 cm^{-1}.

Figure 4 shows two open-beam DTGS spectra acquired by locking-in on the signal generated by phase modulation. The phase modulation method applied to generate these spectra causes the throughput intensity maximum of the spectrum to be shifted towards the near-infrared. In the spectra illustrated, the useful throughput is from 5500 cm^{-1} to about 900 cm^{-1}. To generate these spectra, we accumulated 1024 points with a 300-ms lock-in time constant (signal averaging for 1.1 s), generating 16-cm^{-1} resolution spectra. These two spectra illustrate the dependence of the phase modulation signal on the amplitude of the mirror jitter. This dependence is discussed in further detail below. Spectrum A was generated with a modulation amplitude of 0.320 μm (in optical distance), while spectrum B was generated with an amplitude of 0.080 μm. Although these amplitudes are significantly smaller than needed for optimum modulation of mid-infrared wavelengths, the direct dependence of the signal on the amplitude is easily seen. Figure 5 illustrates the use of phase modulation for transmission spectroscopy with the DTGS detector. This normalized transmission spectrum of a 50-μm polystyrene film was computed from 512 data points measured with the use of a phase modulation amplitude of 0.320 μm and signal averaging for 1.1 s at each point.

Figure 6 compares the *photoacoustic* spectrum of $Na_2[Fe(CN)_5NO]\cdot H_2O$ (sodium nitroprusside) powder detected with the use of (A) relatively weak phase modulation at 600 Hz, (B) amplitude modulation at 100 Hz, and (C) rapid scanning at 120–1500 Hz. The relative intensities of the OH stretching bands centered at 3630 cm^{-1} and 3552 cm^{-1} in these unnormalized spectra illustrate the differences of these modulation techniques. The phase modulation spectrum emphasizes the high energy end of the spectrum, the amplitude modulation spectrum is intermediate, while the rapid scanning spectrum is diminished greatly at high energy. Conversely, the phase modulation spectrum at this amplitude has no useful intensity below 900 cm^{-1}, while the amplitude modulation and rapid scanning spectra are useful to 400 cm^{-1}.

DISCUSSION

In rapid scanning FT-IR-PTS, the photothermal modulation frequency is directly proportional to the wave-

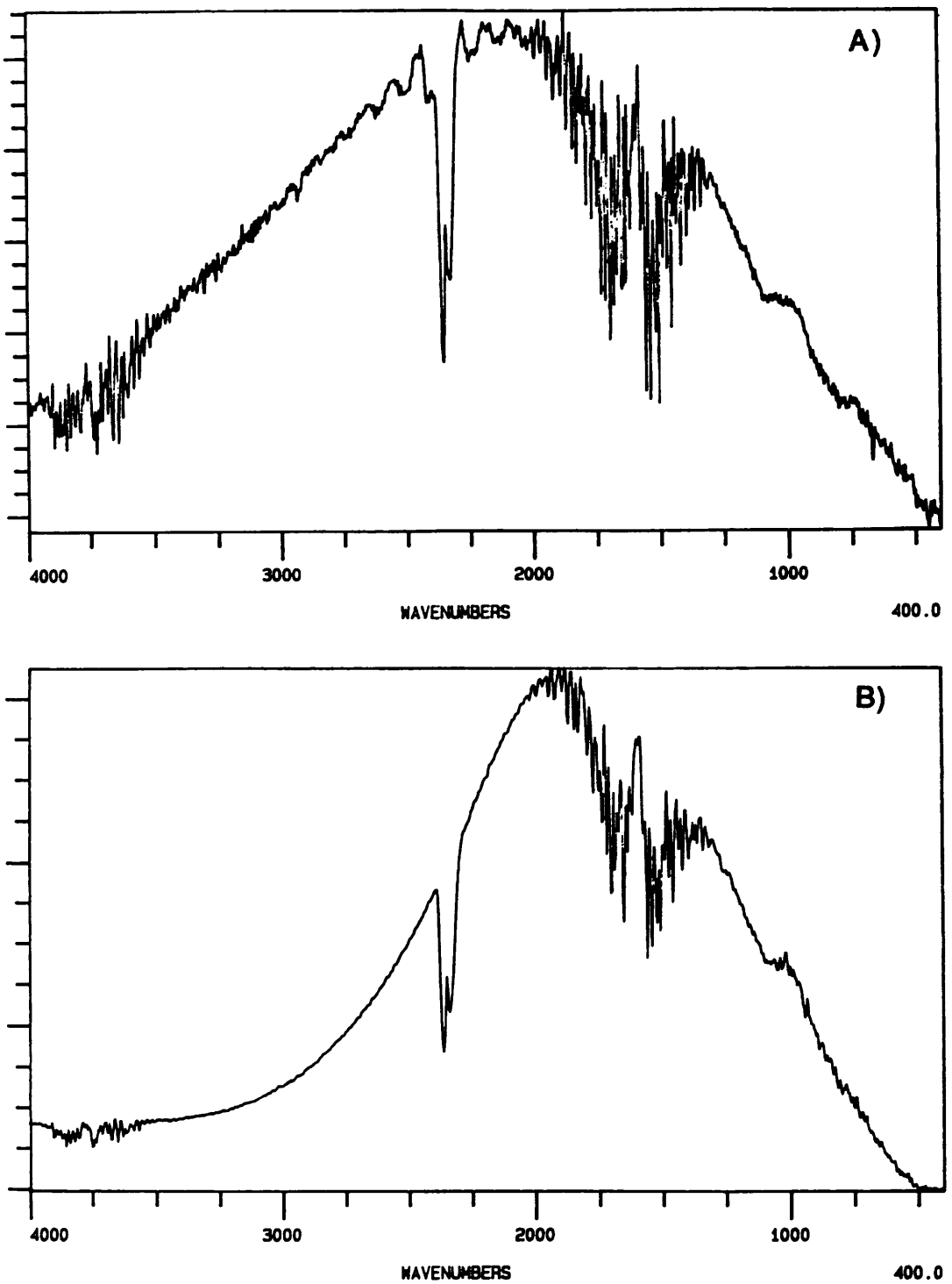

FIG. 3. Photoacoustic spectra of carbon black powder: (A) step scanning with amplitude modulation, 50 Hz; (B) rapid scanning with modulation range, 1500–120 Hz.

number. For example, the PT modulation frequency at 4000 cm^{-1} is 10× that at 400 cm^{-1}. However, the inverse dependence of the signal intensity on wavenumber that this would produce is essentially cancelled by the dependence of the signal on photon energy.[16] Therefore, the resulting FT-IR-PTS spectrum of a blackbody absorber such as carbon black closely resembles the open-beam spectrum of other infrared detectors, because they are essentially source intensity profiles. In any event, normalization of the PT spectrum by ratioing against the spectrum of carbon black is standard practice.

However, although the variation of the modulation frequency with wavenumber in rapid scanning FT-IR-PTS does not cause a problem with signal strength, its effect on the thermal diffusion length in the sample, μ_s, remains a problem since $\mu_s = (a_s/\pi f)^{1/2}$ (where α_s is the thermal diffusivity and f is the modulation frequency in Hz).[16] For example, the effective PT probe depth at 4000

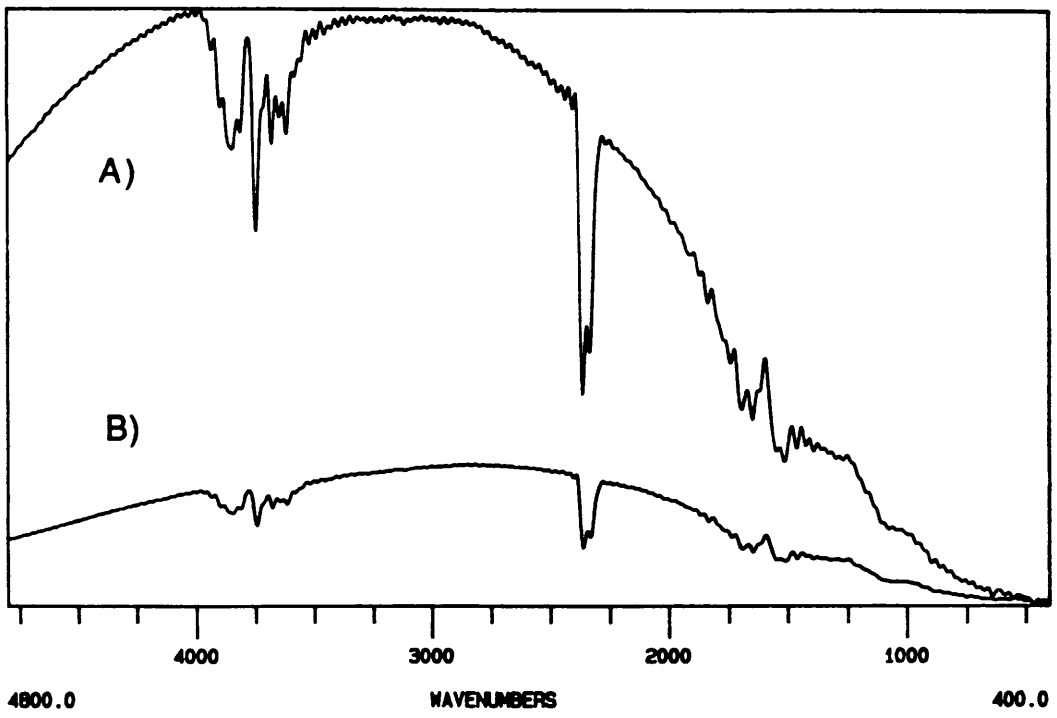

FIG. 4. Phase modulation open-beam DTGS spectra, 600 Hz: (A) 0.320-μm and (B) 0.080-μm phase modulation amplitude.

cm^{-1} is only about $\frac{1}{3}$ that at 400 cm^{-1} for a *homogeneous* sample. This will cause a significant and unpredictable distortion of the relative intensities of bands in the spectra of *heterogeneous* samples and seriously complicate efforts to obtain absorption coefficients from PT data. Vidrine originally suggested generating a composite spectrum of essentially constant modulation frequency by measuring the spectrum with forty different mirror velocities.[2] A simpler approach was suggested by Teng and Royce,[8] which involves measuring the spectrum at two modulation frequencies and then calculating an empirical correction. However, this method is only valid for homogeneous samples and for samples for which the photoacoustic contribution due to thermal expansion of gases in the interstitial layers is negligible. Recently, others have suggested the use of photoacoustic phase analysis to determine absorption coefficients.[17-20] These methods are promising but, for FT-IR, could be greatly simplified

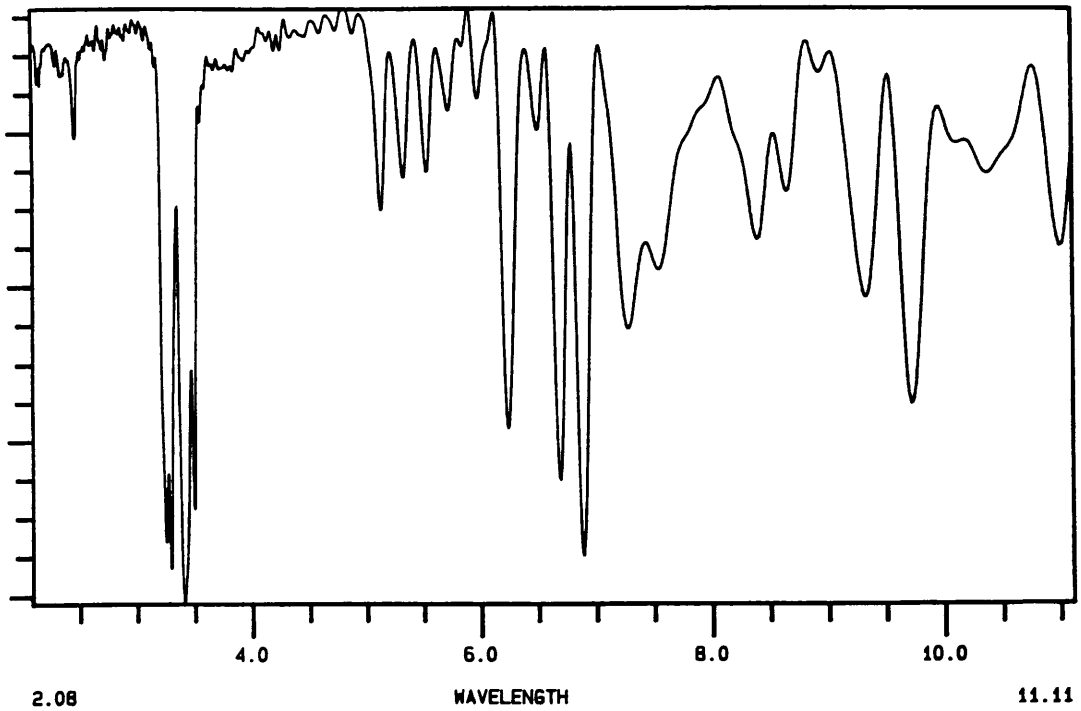

FIG. 5. Transmission spectrum of standard 50-μm polystyrene sample; phase modulation, 600 Hz, with 0.320-μm amplitude.

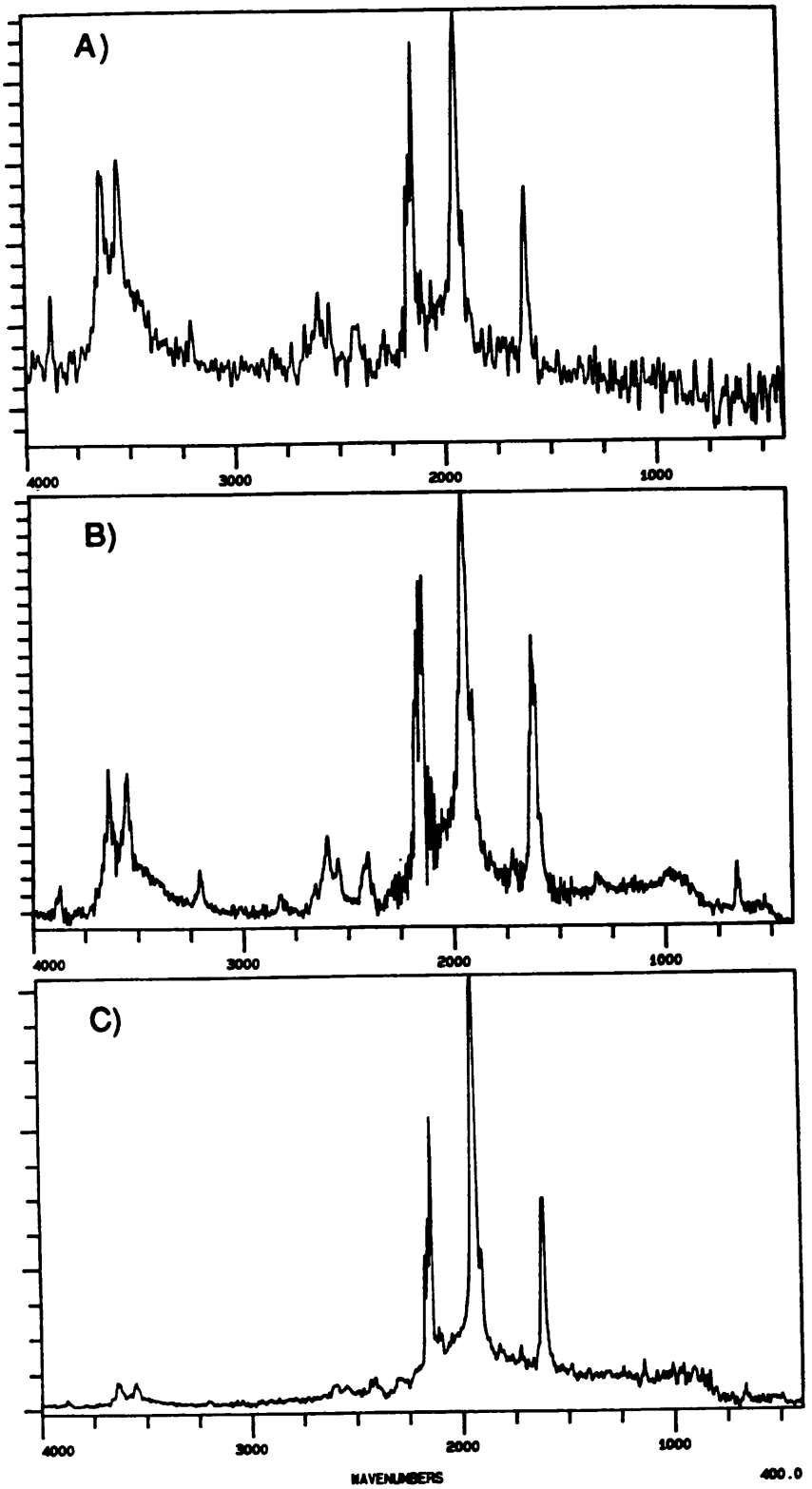

FIG. 6. Photoacoustic spectra of sodium nitroprusside powder: (A) step scanning with phase modulation at 600 Hz, with 0.320-μm amplitude; (B) step scanning with amplitude modulation at 200 Hz; (C) rapid scanning with modulation range, 1500–120 Hz.

if the modulation frequency, and hence the thermal diffusion length, were constant over the whole spectral range.

Although standard rapid scan methods have been used for all FT-IR-PAS and PTS to date, constant (synchronous) modulation superimposed on the rapid scan interferogram has been the key to realization of two other FT-IR techniques: polarization modulated IRRAS (IR reflection adsorption spectroscopy)[21] and FT-VCD (FT vibrational circular dichroism).[22] Because of the standard fast IR detectors used with these techniques, the high modulation frequencies (~50 kHz) necessary for effective demodulation in the presence of the Fourier fre-

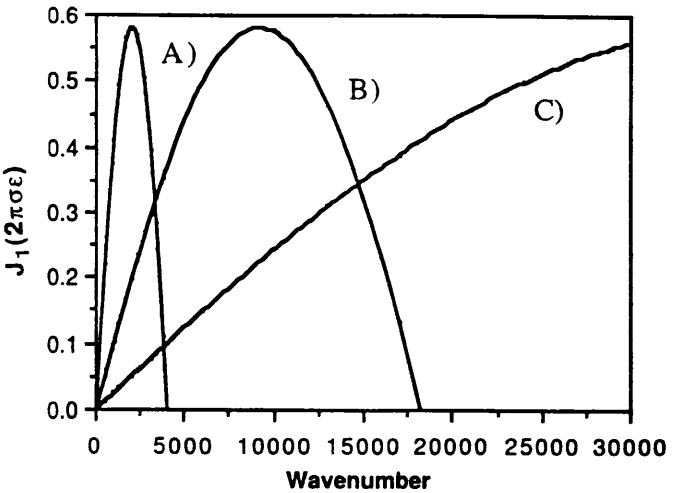

FIG. 7. Phase modulation characteristics for modulation amplitudes of: (A) 1.45 μm, (B) 0.320 μm, (C) 0.080 μm.

quencies pose no problem (and, in fact, are an advantage in terms of S/N). However, in order to implement the relatively low modulation frequencies which are essential, for example, for photothermal or other slow detectors, step scanning appears to be the technique of choice for mirror movement, in combination with constant modulation frequency.

As mentioned above, with step scanning, the intensity modulation appropriate for photothermal detection can be generated by either: (1) external (chopper) amplitude modulation (AM), or (2) internal (mirror jitter) phase modulation (PM). Each method has its advantages, but in terms of S/N, PM can be shown—theoretically and practically—to be superior.[12]

The comparison of step scanning with AM (50 Hz) to rapid scanning (both at 8-cm^{-1} resolution) is shown in Fig. 3A and 3B. By the use of carbon black as the sample, the significantly higher photothermal signal intensity at higher energies in the step scan spectrum (owing to the constant modulation) is clearly illustrated. In contrast, in the rapid scan spectrum the modulation frequency increases from 120 Hz at 400 cm^{-1} to 1200 at 4000 cm^{-1} (mirror velocity 0.31 cm s^{-1}), which produces very low PT signal levels above 3000 cm^{-1}.

The step scan spectrum in Fig. 3A was obtained with the use of the vector magnitude output of the Model 5204. Alternatively, a phase analysis can be carried out by measuring the in-phase and quadrature components relative to the chopper reference signal, or, for small phase angles, the phase of the PT signal can be used directly. In either case, the small change in the amplitude of the detected signal is the interferogram used to compute the photoacoustic spectrum.

It should be noted from Fig. 3A and 3B that greater signal strength in the 3000–4000 cm^{-1} region in the step scan spectrum does not, in fact, mean substantially greater S/N. The reasons for this lie in the fundamental nature of amplitude modulation. With AM (using an external chopper), the dynamic range of the measurement is greatly reduced since the detected signal consists of a large "dc" background (which is invariant with path difference and does not contribute to the interferogram) plus a smaller "ac" signal (which is the interferogram). Consequently, the underlying low-frequency fluctuations of the dc signal are amplified along with the desired ac component and appear as noise in the interferogram. These fluctuations can appear as a result of electronic drift, mechanical/optical drift, convection, or small source intensity variation. The consequence is that neither lower frequency modulation (theoretically effective in increasing PT signal strength) nor longer integration times result in the desired S/N improvement. This disadvantage of AM is not shared by PM, which produces the ac signal (the interferogram) without the dc background.

Although there is no dc background, the PM detector signal does vary with wavenumber, depending on the amplitude of mirror jitter.[11,12] For the case of sinusoidal modulation, extension of Eq. 2, to cover all wavelengths, gives the general expression for the PM interferogram,

$$I(\delta) = \int_0^\infty B(\sigma)\cos(2\pi\sigma(\delta + \epsilon \sin \omega t))\, d\sigma. \quad [4]$$

This can be expanded to yield:

$$I(\delta) = \int_0^\infty B(\sigma)[\cos(2\pi\sigma\delta)\cos(2\pi\sigma\epsilon \sin \omega t) - \sin(2\pi\sigma\delta)\sin(2\pi\sigma\epsilon \sin \omega t)]\, d\sigma, \quad [5]$$

where σ is the energy of the light (cm^{-1}). The two components of the Fourier integrand can be further expanded in terms of Bessel functions J_x as follows:

$$\cos(2\pi\sigma\epsilon \sin \omega t) = J_0(2\pi\sigma\epsilon) - 2J_2(2\pi\sigma\epsilon)\sin 2\omega t + 2J_4(2\pi\sigma\epsilon)\sin 4\omega t - \ldots \quad [6]$$

and

$$\sin(2\pi\sigma\epsilon \sin \omega t) = 2J_1(2\pi\sigma\epsilon)\sin \omega t - 2J_3(2\pi\sigma\epsilon)\sin 3\omega t + \ldots. \quad [7]$$

If a lock-in amplifier is tuned to accept the component at the fundamental frequency, then only the $2J_1(2\pi\sigma\epsilon)\sin \omega t$ term is significant, and demodulation of the signal at ω gives the phase modulation interferogram:

$$I(\delta) = \int_0^\infty B'(\sigma)2J_1(2\pi\sigma\epsilon)\sin 2\pi\sigma\delta\, d\sigma. \quad [8]$$

Thus, the PM interferogram (in the absence of phase errors) is antisymmetric with respect to zero path difference and (in the limit of infinitely small phase modulation amplitude) is the derivative of the AM interferogram. In addition, the integrand is convolved with the first-order Bessel function, $J_1(2\pi\sigma\epsilon)$, and thus depends on the product of the modulation amplitude and the energy of the light.

Chamberlain has referred to the function $J_1(2\pi\sigma\epsilon)$ as the "phase modulation characteristic."[12] The first-order Bessel function rises from zero (when the argument $2\pi\sigma\epsilon$ is zero), reaches a maximum when the argument is 0.58π, and then falls through zero again, to become negative at $2\pi\sigma\epsilon = 3.84$. Thus, the phase modulation characteristic has its first (and principal) maximum at $\sigma\epsilon = 0.29$, and its first zero occurs at $\sigma\epsilon = 0.61$. Figure 7 shows the phase modulation characteristic as a function of wavenumber, σ, for several values of ϵ, the phase modulation amplitude.

As shown in Fig. 7, when a very small modulation

amplitude is selected, only frequencies of very high energy are significantly modulated. In fact, with a modulation amplitude of 0.080 μm, as illustrated in Fig. 4B, the phase modulation characteristic is maximized at an energy of 36,250 cm^{-1}, in the ultraviolet. With an increase in the modulation amplitude to 0.320 μm, as in Fig. 4A, the phase modulation characteristic maximum shifts to lower energy (9063 cm^{-1}), and correspondingly longer wavelengths are more strongly modulated. Thus, in spite of the fact that the instrument throughput is decreasing at energies above 2000 cm^{-1}, the spectrum in Fig. 4A shows a signal maximum near 4000 cm^{-1} due to the increase in modulation as the wavenumber approaches the phase characteristic maximum value. Above 4000 cm^{-1}, however, the low throughput dominates, and the signal begins to decrease.

Clearly, the amplitude of the phase modulation can be used to optimize the performance of the step scan interferometer for any desired wavelength. For example, optimizing the phase modulation characteristic for 2000 cm^{-1} (i.e., with a phase modulation amplitude of 1.45 μm), would increase the signal strength at 2000 cm^{-1} by a factor of ~3 relative to the result in Fig. 4A (see Fig. 7). However, phase modulation of such an amplitude is a problem because the optimal phase modulations used for mirror control and signal generation are very different.

Mirror positional noise is minimized by the use of a very small mirror jitter amplitude for control. That is to say, the uncertainty in average position at any one sampling point is directly related to the amplitude of the modulation about that point. For example, in the current instrument, the observed noise on the laser control signal when the PM is ±8 nm and the control frequency is 600 Hz indicates that the short-term positional uncertainty is only ±2 nm, which is $\lambda_{HeNe}/300$. On the other hand, when the PM is ±46 nm, the error corresponding to the observed noise is ±16 nm, or $\lambda_{HeNe}/40$. (As long as, on average, the mirror is displaced evenly on either side of the desired sampling point, signal averaging will further reduce the total positional error at each sampling point by a factor of $(t)^{1/2}$, where t is the time of averaging.) Finally, it is observed that mirror control is best accomplished with PM frequencies above 500 Hz.

Although higher modulation frequencies and lower modulation amplitudes are advantageous for mirror position control, as pointed out above, for PT spectroscopy, the signal is inversely proportional to the modulation frequency and directly proportional to the depth of modulation. Thus, although the PM used for mirror control can be used to generate the photothermal signal at the shorter NIR/VIS wavelengths,[9] optimum modulation for the mid-IR requires higher modulation amplitudes and lower modulation frequencies than those used for best mirror control. Thus, for maximum versatility, the two-phase modulations should be independently generated.

The application of PM step scan FT-IR-PAS to the measurement of the spectrum of $Na_2Fe(CN)_5NO \cdot H_2O$ powder and the comparison with the results obtained by AM step scanning, as well as by rapid scanning (Fig. 6A, 6B, 6C) further illustrate the points discussed above. Because of instrumental limitations at the time of this report, the phase modulation used to generate the signal is the same as that used to control the mirror. For this reason, it is necessarily much lower in amplitude and higher in frequency than is optimal for IR modulation. Although in Fig. 6 the S/N in the PM spectrum is less than that in the AM spectrum, these results, along with those illustrated in Fig. 4A and 4B, clearly indicate that an increase in amplitude to 1.45 μm (required to maximize the phase characteristic at 2000 cm^{-1}), along with a reduction in frequency to, say, 100 Hz, would bring about a dramatic improvement. First is the factor due to the ratio of the phase modulation characteristic for 0.320 μm vs. 1.45 μm at 2000 cm^{-1} (Fig. 7). This is approximately 4×. Second is the dependence of the PA signal strength on modulation frequency, which is between ω^{-1} and $\omega^{-3/2}$. This will give a factor of approximately 6× in this case, therefore predicting an improvement of ~25× in signal strength. The theoretical prediction is that PM will give ~2.5× better S/N than will AM, in the case of detector-limited noise.[12] In our experiments the noise is apparently not detector limited, and thus PM produces an improvement in S/N that is even larger than the theoretical prediction.[23]

It should be noted that the question of positional uncertainty is more critical in step scanning (where the mirror must be essentially stopped at each data point) than in rapid scanning (where the mirror is driven at constant velocity). In step scanning, the feedback mechanism which holds the mirror in position must be able to react to random environmental stresses by applying counter voltages in *either* direction of mirror motion. A key point is that the step scan system relies on this feedback mechanism to ensure that the sampling interval remains constant. With rapid scanning, on the other hand, the feedback mechanism reacts only to speed up or slow down the mirror, by decreasing or increasing the drive voltage, and thus keeping the velocity constant. However, regardless of whether the velocity remains exactly constant, the laser referencing system ensures that data are sampled at constant intervals of retardation (Conne's advantage). Thus, the effectiveness of the feedback mechanism for step scanning is far more critical than it is for rapid scanning.

In addition, there are other sources of noise which the rapid scanning instrument is better able to reject, since the noise is of low frequency relative to the Fourier modulation frequencies (and therefore is Fourier transformed out of the spectral energy range of interest). These include source fluctuations (both spatial and intensity), nonuniformity of detector response with time, and electronic gain drift. However, with proper attention to instrument design, including thermostating, and/or evacuation of the optics bench, these sources of noise can be minimized.

Despite the difficulties, the potential advantages of step scanning for slow detector response techniques, such as photothermal methods, make perfecting the step scan FT spectrometer worthwhile. Step scan methods have already proven to be of great value for photothermal spectroscopy at shorter wavelengths.[9] In addition, recent extension of photothermal measurements into the far-infrared[24] may also benefit from the modulation frequency control and lock-in detection afforded by the step scan technique in this energy-starved region of the spec-

trum. Finally, an additional potentially very valuable use of step scan FT-IR is infrared time-resolved spectroscopy (TRS).[25] In this application, at each step of the interferometer an event is triggered (for example, by a short laser or electrical pulse), and the time evolution of the interferometer output, as modified by the sample, is recorded by a transient digitizer. Subsequently, the data may be sorted by time, and then Fourier transformed to produce a time-ordered sequence of spectra. The primary advantage of step scanning in this case is that it imposes no limitations on the time-scale of events observed, in contrast to rapid scan TRS techniques.[25]

As pointed out above, in order to maximize the versatility of the step scan interferometer so that it can be used effectively in any region of the spectrum, the mirror control and interferometer-beam modulation parameters should be independently adjustable. This can be accomplished by separating the phase modulation of the infrared radiation from the HeNe laser control by using two independent mirrors in the "fixed"-pathlength arm of the interferometer. The smaller of the two mirrors is mounted rigidly to the support plate in the fixed arm and is used to reflect only the laser radiation. As in the present configuration of the interferometer, one accomplishes weak phase modulation of the laser signal by jittering the *mirror*, using the existing feedback control circuitry. To modulate the infrared beam, one mounts the second, larger mirror in the "fixed"-pathlength arm to a piezoelectric transducer, which is in turn mounted to the interferometer support plate. A modulated power supply connected to the piezoelectric transducer is then used to generate phase modulation of the infrared radiation, at any desired frequency and amplitude, independent of the laser control signal. These and other instrument modifications are in progress in our laboratory.

ACKNOWLEDGMENTS

This work has been supported in part by grants from NATO (Collaborative Research Grant No. 86/0791), the U.S.-EPA (Research Assistance Grant No. CR813023-02-0), and the Duke University Research Council, as well as by loan of equipment from the IBM Corporation. The authors also wish to acknowledge the extensive advice and consultation of Professor A. Claude Boccara and Dr. Danièle Fourier.

1. M. G. Rockley, Chem. Phys. Lett. **68**, 455 (1979).
2. D. W. Vidrine, Appl. Spectrosc. **34**, 314 (1980).
3. J. W. Childers and R. A. Palmer, Am. Lab. **18 (3)**, 22 (1986).
4. M. A. Martin, J. W. Childers, and R. A. Palmer, Appl. Spectrosc. **41**, 120 (1987).
5. (a) M. J. D. Low, M. Lacroix, and C. Morterra, Spectrosc. Lett. **15**, 57 (1982); (b) M. J. D. Low and C. Morterra, Appl. Spectrosc. **41**, 280 (1987).
6. R. A. Palmer and M. J. Smith, Can. J. Phys. **64**, 1086 (1986).
7. M. E. Peoples, M. J. Smith, and R. A. Palmer, Appl. Spectrosc. **41**, 1257 (1987).
8. Y. C. Teng and B. S. H. Royce, Appl. Opt. **21**, 77 (1982).
9. D. Débarre, A. C. Boccara, and D. Fournier, Appl. Opt. **20**, 4281 (1981).
10. D. Débarre, Thèse, Docteur 3ème Cycle, Université de Paris-sud, Centre d'Orsay (1981).
11. (a) J. Chamberlain, Infrared Phys. **11**, 25 (1971); (b) J. Chamberlain and H. A. Gebbie, Infrared Phys. **11**, 57 (1971).
12. J. W. Chamberlain, *Principles of Interferometric Spectroscopy* (John Wiley & Sons, New York, 1979).
13. L. Lloyd, S. M. Riseman, R. K. Burnham, E. M. Eyring, and M. M. Farrow, Rev. Sci. Instrum. **51**, 1488 (1980).
14. J. Connes and P. Connes, J. Opt. Soc. Am. **56**, 896 (1966).
15. P. L. Richards, J. Opt. Soc. Am. **54**, 1474 (1964).
16. A. Rosencwaig and A. Gersho, J. Appl. Phys. **47**, 64 (1976).
17. J. C. Roark, R. A. Palmer, and J. S. Hutchison, Chem. Phys. Lett. **60**, 112 (1978).
18. M. Choquet, G. Rousset, and L. Bertrand, Can. J. Phys. **64**, 1081 (1986).
19. S. J. McGovern, B. S. H. Royce, J. B. Benziger, J. Appl. Phys. **57**, 1710 (1985).
20. B. S. H. Royce, Plenary Lecture WP1, 5th International Topical Meeting on Photoacoustic and Photothermal Phenomena, Heidelberg, F.R.G. (1987).
21. W. G. Golden, D. D. Saperstein, M. W. Severson, and J. Overend, J. Phys. Chem. **88**, 572 (1984).
22. L. A. Nafie and D. W. Vidrine, in *Fourier Transform Infrared Spectroscopy*, J. R. Ferraro and L. J. Basile, Eds. (Academic Press, New York, 1982), Vol. 3, pp. 83–123.
23. C. J. Manning, M. J. Smith, R. A. Palmer, and J. L. Chao, unpublished results.
24. R. J. Rosenthal, 14th Annual Meeting of the Federation of Analytical Chemistry and Spectroscopy Societies (1987), Paper 451.
25. W. M. Grim III, J. A. Graham, R. M. Hammaker, and W. G. Fateley, Am. Lab. **16 (3)**, 22 (1984).